THE JOURNAL OF BIOLOGICAL CHEMISTRY Vol. 277, No. 50, Issue of December 13, pp. 48849–48857, 2002

A New Level of Conotoxin Diversity, a Non-native Disulfide Bond Connectivity in α-Conotoxin AuIB Reduces Structural Definition but Increases Biological Activity*

Received for publication, August 29, 2002, and in revised form, October 4, 2002
Published, JBC Papers in Press, October 9, 2002, DOI 10.1074/jbc.M208842200

Julie L. Dutton‡§, Paramjit S. Bansal‡, Ron C. Hogg¶, David J. Adams¶, Paul F. Alewood‡, and David J. Craik‡‖

From the ‡Institute for Molecular Bioscience and ¶School of Biomedical Sciences, Department of Physiology and Pharmacology, University of Queensland, Brisbane, Queensland 4072, Australia

α-Conotoxin AuIB and a disulfide bond variant of AuIB have been synthesized to determine the role of disulfide bond connectivity on structure and activity. Both of these peptides contain the 15 amino acid sequence GCCSYPPCFATNPDC, with the globular (native) isomer having the disulfide connectivity Cys(2–8 and 3–15) and the ribbon isomer having the disulfide connectivity Cys(2–15 and 3–8). The solution structures of the peptides were determined by NMR spectroscopy, and their ability to block the nicotinic acetylcholine receptors on dissociated neurons of the rat parasympathetic ganglia was examined. The ribbon disulfide isomer, although having a less well defined structure, is surprisingly found to have approximately 10 times greater potency than the native peptide. To our knowledge this is the first demonstration of a non-native disulfide bond isomer of a conotoxin exhibiting greater biological activity than the native isomer.

The main component of the venom of cone snails, carnivorous mollusks from tropical marine environments, is a group of disulfide-rich peptides that act as potent and highly specific antagonists of ion channels and receptors (1–3). These channels and receptors play vital physiological roles, and envenomation results in rapid immobilization of prey. One family of these peptides is the α-conotoxins, which target nicotinic acetylcholine receptors (nAChRs)[1] in skeletal muscle and neurons (4–6). These peptides are just 12–18 amino acids in length and feature four conserved cysteine residues.

As is depicted in Fig. 1, the four cysteine residues may, in principle, be joined to form disulfide bonds in three different ways, resulting in formation of "globular," "ribbon," and "beads" disulfide bond isomers. In nature the α-conotoxins are present exclusively in the globular form, raising the following question: "What are the advantages of this linkage pattern compared with the two other possibilities?" Their relative ease of synthesis, the small number of possible disulfide bond isomers, and their structural definition (7–17) make α-conotoxins ideal model peptides for the study of the effects of disulfide bonding on protein structure, which in turn may lead to answers to this question.

The cysteine framework (*i.e.* the placement and spacing of cysteine residues within the peptide sequence) of the α-conotoxins is highly conserved and correlates with their functional and structural features. The first and second cysteines in α-conotoxins are always adjacent to one another, but the number of residues between the second and third cysteines and between the third and fourth cysteines varies (Fig. 1). Based on the intracysteine loop spacing the toxins are divided into four framework classes, with loop spacings of 3/5, 4/3, 4/6 or 4/7. All of the 3/5 α-conotoxins antagonize muscle nAChRs, whereas the 4/*X* classes, with the exception of EI, are active against the neuronal nAChRs (Table I). The difference in the functions of the classes is reflected in distinct differences between their sequences and three-dimensional structures. Whereas all of the α-conotoxins feature a central helix flanked by turns, the helix is 3_{10} in 3/5 α-conotoxins and takes an α configuration in members of the 4/*X* classes.

The 3/5 α-conotoxin GI and derivatives thereof have been used recently to examine the cooperative formation of disulfide bonds (18). GI, and related 3/5 α-conotoxins GII and MI, have been used in studies concerned with determining the effect of changes to the number or connectivity of disulfide bonds on peptide function (19–21). Gehrmann *et al.* (22) determined the NMR solution structures of the three possible disulfide bond isomers of GI and found considerable structural variations among them. Whereas the globular form exhibited a single well defined conformation in solution, the ribbon and beads isomers displayed an increasing degree of conformational heterogeneity. The connectivity of the disulfides in the beads isomer so dramatically reduced the stability of the structure that a single superposition of the ensemble of NMR structures was not possible.

Zhang and Snyder (23) have shown that the spacings of the cysteines can affect the preferred disulfide connectivity of α-conotoxins. In their study, they oxidized GI and various mutants of GI, including Pro-5 → Ala GI mutants with or without residues Cys-7 and Ala-6 swapped. Oxidation of the GI analogues, in both denaturing and folding solvents, and the sub-

* This work was supported in part by a grant from the Australian Research Council. The costs of publication of this article were defrayed in part by the payment of page charges. This article must therefore be hereby marked "*advertisement*" in accordance with 18 U.S.C. Section 1734 solely to indicate this fact.

The atomic coordinates and structure factors (code 1MXN and 1MXP) have been deposited in the Protein Data Bank, Research Collaboratory for Structural Bioinformatics, Rutgers University, New Brunswick, NJ (http://www.rcsb.org/).

§ Supported by an Australian Postgraduate award.

‖ ARC Professorial Fellow. To whom correspondence should be addressed: Institute for Molecular Bioscience, University of Queensland, Brisbane, Queensland 4072, Australia. Tel.: 61-7-3365-4945; Fax: 61-7-3365-2487; E-mail: d.craik@imb.uq.edu.au.

[1] The abbreviations used are: nAChR, nicotinic acetylcholine receptor; NMR, nuclear magnetic resonance; HPLC, high performance liquid chromatography; Mebzl, methyl benzyl; MS, mass spectrometry; DQF-COSY, double quantum filtered correlation spectroscopy; ECOSY, exclusive correlation spectroscopy; TOCSY, total correlation spectroscopy; NOESY, nuclear Overhauser spectroscopy; NOE, nuclear Overhauser effect; RMSD, root mean square deviation; ACh, acetylcholine; HF, hydrogen fluoride; ppb, parts per billion.

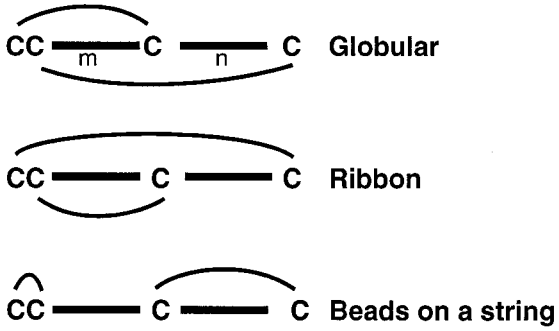

FIG. 1. **α-Conotoxin framework.** The number of residues between the second and the third cysteines (referred to as loop 1) and between the third and the fourth cysteines (referred to as loop 2) are represented by "*m*" and "*n*," respectively. α-Conotoxin framework classes are defined by *m* and *n*, with the 3/5 class, for example, having three residues in loop 1 and five residues in loop 2, exemplified by the α-conotoxin GI. The three theoretically possible disulfide bond isomers are illustrated.

sequent analysis of the resulting isomers by high performance liquid chromatography (HPLC) revealed that shortening the first loop of the framework from three to two non-cysteine residues resulted in a reversal of the preferences for different isomers. Mutation of the proline to an alanine did not affect the preferences. They concluded that an even number of residues in a loop is preferred over an odd number of residues for loop sizes of fewer than five residues. This conclusion is consistent with earlier studies in which they examined the formation of a single disulfide bond in small peptides containing two cysteines separated by different numbers of amino acid residues (24).

In general, studies of disulfide bonding in α-conotoxins have been confined to the 3/5 class. It was of interest to examine the effects of disulfide bonding on structure in α-conotoxins from different framework classes because of the significant effects of cysteine spacing on disulfide bonding preferences seen in model systems and the differences in structure and function between the various α-conotoxin classes. Such studies are given further impetus by the fact that new families of conotoxins with alternative disulfide connectivities are now being found. For example a new family of conotoxins that displays the ribbon disulfide connectivity as their native form has been isolated recently (25–27). These molecules, referred to as χ or λ-conotoxins, are of similar size but exhibit different biological activity, primary sequences, and cysteine spacings to the α-conotoxins (Table I).

The observed preference for globular disulfide bond connectivity over the ribbon and beads forms in 3/5 α-conotoxins is consistent with the rules established by Zhang and Snyder (23). By applying the same rules to the 4/*X* α-conotoxins, it is clear that the globular and ribbon forms would be preferred over the beads isomer. A disulfide bond between adjacent cysteines is energetically unfavorable. The reason for the absolute preference for the globular connectivity over the ribbon connectivity in 4/*X* α-conotoxins is not obvious from analysis of cysteine spacings. As is shown in Table II, small conotoxins with 4/*X* spacings may exhibit either globular or ribbon disulfide bond connectivities in their native forms.

In this paper we report the chemical synthesis and NMR solution structures of the globular (native) and ribbon disulfide bond isomers of a 4/6 α-conotoxin, AuIB (28). We also report the finding that the AuIB ribbon isomer has 10-fold greater activity in dissociated neurons of rat parasympathetic ganglia than native AuIB, and we consider this in light of the structural data. Although some studies have looked at the function of α-conotoxins with altered numbers or arrangements of disulfide bonds, none of these studies included members of the 4/6 or 4/7 classes (19–21). In those classes the reason for the preference for globular connectivity over ribbon connectivity is unclear. In addition, although activity of some α-conotoxins has been increased through mutation of specific residues, there have been no previous reports of an increase in biological activity as a result of altering disulfide bond connectivity from native.

EXPERIMENTAL PROCEDURES

Peptide Synthesis—The peptides were assembled on Boc-Phe-OCH_2-Pam resin using standard BOC chemistry. A linker, 4-(α-*tert*-butoxycarboxylaminobenzyl) phenoxyacetic acid, was attached to the resin to form the C-terminal amide. The amino acids Boc-Ala, Asn(Xan), Asp(O-cHex), Cys(methylbenzyl (Mebzl)), Gly, Phe, Pro, Ser(Bzl), Thr(Bzl), and Tyr(BrZ) were obtained from Auspep (Melbourne, Australia). All reagents were of synthesis or HPLC grade.

AuIB globular and ribbon isomers were synthesized using MeBzl-protecting groups on the cysteines. The assembled peptides were cleaved from the resin using liquid hydrogen fluoride (HF)/*p*-cresol/*p*-thiocresol (18:1:1) at 0–2 °C for 2 h. The crude peptides were purified on a Vydac C18 column, with a gradient of 1% B per min (A = 0.1% trifluoroacetic acid in H_2O, B = 0.09% trifluoroacetic acid in 90% acetonitrile/H_2O). Pure peptide, assessed by analytical C18 HPLC and electrospray mass spectrometry (MS), was prepared. The MeBzl protecting groups were removed in the HF cleavage reaction. The globular and ribbon isomers were formed by oxidation of the fully reduced peptide at a concentration of 0.08 mg/ml in 20% isopropyl alcohol in 0.1 M NH_4HCO_3 (pH 8.0). The oxidized peptides were purified by preparative C18 HPLC.

NMR—Samples for NMR experiments contained ~2.0 mM peptide in either ^2H_2O or 90% H_2O/10% ^2H_2O at pH 3.5. The pH values are meter readings at 295 K that were uncorrected for deuterium isotope effects. NMR experiments were carried out on Bruker 500 and 750 MHz NMR spectrometers. These included double quantum-filtered correlation spectroscopy (DQF-COSY) (29), exclusive correlation spectroscopy (ECOSY) (30), total correlation spectroscopy (TOCSY) with a mixing time of 80 ms (31), and nuclear Overhauser effect spectroscopy (NOESY) with mixing times of 150, 200, 350, and 400 ms (32–33). Spectra were routinely acquired at 280 and 290 K. They were internally referenced to sodium 2,2-dimethyl-2-silapentane-5-sulfonate at 290 K after acquisition of all other experiments.

Identification of slowly exchanging amide protons was achieved by acquisition of one-dimensional and TOCSY spectra immediately upon dissolution of fully protonated peptide in ^2H_2O. Additional information for the backbone NH resonances was acquired from one-dimensional spectra in 90% H_2O, 10% ^2H_2O recorded at 280, 285, 290, 295, and 300 K for both the globular and ribbon forms and also at 297.5, 302.5 and 305 K for the globular form. This information was used to determine NH temperature coefficients. Additional spectra were acquired using samples of globular AuIB at pH 2.6, 4.2, and 6.8.

Spectra were processed on a Silicon Graphics Indigo Workstation using XWIN-NMR (Bruker).

Structure Determination—Nuclear Overhauser effect (NOE) restraints were derived from the intensity of cross-peaks in 150- or 200-ms NOESY spectra. The restraints were derived from 280 and 290 K experiments for the ribbon and native isomers, respectively. They were classed as either strong (1.8–2.7 Å), medium (1.8–3.5 Å), weak (1.8–5.0 Å), or very weak (1.8–6.0 Å) (34, 35). Pseudo-atom corrections of 1.5 Å for methyl, 1.0 Å for methylene, and 2.0 Å for tyrosine ring protons were added (36).

$^3J_{HNH\alpha}$ couplings were measured from DQF-COSY spectra. Backbone ϕ dihedral restraints of $-65 \pm 15°$ were applied for $3 \leq {}^3J_{HNH\alpha} \leq 5.8$ Hz and $-120 \pm 30°$ for $8 \leq {}^3J_{HNH\alpha} \leq 9.5$ Hz.

$^3J_{H\alpha H\beta 1}$ and $^3J_{H\alpha H\beta 2}$ coupling constants were measured from ECOSY spectra of the peptide in ^2H_2O. Consideration of the coupling constants and NOE intensities allowed inclusion of $\chi 1$ angle restraints and stereospecific assignment of β carbon protons. χ_1 angles restraints of $180 \pm 30°$ for a "t" conformation around the Cα–Cβ bond (NH-Hβ2 NOE = strong/medium, NH-Hβ1 NOE = strong, Hα-Hβ2 NOE = strong, Hα-Hβ1 NOE = weak, $^3J_{H\alpha H\beta 2} < 5$ Hz, and $^3J_{H\alpha H\beta 1} > 10$ Hz) and χ_1 angles of $-60 \pm 30°$ for a "g^+" conformation around the Cα–Cβ bond (NH-Hβ2 NOE = strong, NH-Hβ1 NOE = weak, Hα-Hβ2 NOE = weak, Hα-Hβ1 NOE = strong, $^3J_{H\alpha H\beta 1} < 5$ Hz, and $^3J_{H\alpha H\beta 2} > 10$ Hz) were included as restraints.

Three-dimensional structures were calculated using simulated annealing and energy minimization protocols in X-PLOR (37, 38) as described previously (39). NOE distance and dihedral angle restraints for the globular and ribbon isomers were used in X-PLOR version 3.851 to

TABLE I

Representatives of the α-, ε-, ρ-, and χ/λ conotoxin families

Cysteines involved in disulfide bonds are in boldface type. ND, not determined; e, carboxyglutamic acid; w, bromotryptophan; t, threonine with a linked *N*-acetylgalactosamine-galactose disaccharide; O, hydroxyproline; ∗, amidated C terminus.

Name	Sequence	Receptor[a]	DiS[b]	m/n[c]	F[d]	Ref.
GI	E**CC**-NPA**C**GRHYS–**C**∗	M $(\alpha1)_2$ $\beta\gamma\delta$	G	3/5	α	53
EI	RDO**CC**YHPT**C**NMSNPQ**IC**∗	M $(\alpha1)_2$ $\beta\gamma\delta$	G	4/7	α	54
PnIA	G**CC**SLPP**C**AANNPDY**C**∗	N α3 β2	G	4/7	α	55
EpI	G**CC**SDPR**C**NMNNPDY**C**∗	N α3 β2/α3 β4	G	4/7	α	56
MII	G**CC**SNPV**C**HLEHSNL**C**∗	N α3 β2	G	4/7	α	57
AuIB	G**CC**SYPP**C**FATNPD-**C**∗	N α3 β4	G	4/6	α	28
ImI	G**CC**SDPRCAWR—**C**∗	N α7	G	4/3	α	58
TxIX	e**CC**eDGw**C**——**C**tAAO	ND	G	4/0	ε	59
TIA	FNWR**CC**LIPACRRNHKKF**C**∗	α_1-Adrenoceptor	G	4/7	ρ	25
MrIA	NGV**CC**GYKLCHO——C	NET	R	4/2	χ/λ	25–27

[a] M, muscle nicotinic acetylcholine receptor; N, neuronal nicotinic acetylcholine receptor; NET, noradrenaline transporter.
[b] DiS, disulfide connectivity.
[c] *m* and *n* refer to the number of residues between the second and third cysteine and between the third and fourth cysteine.
[d] F, family.

TABLE II

Loop sizes of the three possible disulfide bond isomers fo r different framework classes of conotoxin

G, R, and B refer to globular, ribbon, and bead disulfide bond connectivities, respectively. In the abbreviation for the framework given in the boxheads, *m*/*n*, *m* refers to the number of residues between the 2nd and 3rd Cys, and *n* refers to the number of residues between the 3rd and 4th Cys. The framework (*m*/*n*) is written in italic type and roman type for α-conotoxin and other small conotoxin frameworks, respectively. Loop spacing is abbreviated in the body of the table as *x*:*y* where *x* is the number of residues between the 1st Cys and the Cys it is disulfide-bonded to, and *y* is the number of residues between the Cys residues that form the other disulfide bond. The loop spacing found in the native peptides is written in boldface type.

	Framework (*m*/*n*)					
	3/5	4/0	4/2	*4/3*	*4/6*	*4/7*
G	**4:9**	**5:5**	5:7	**5:8**	**5:11**	**5:12**
R	10:3	6:4	**8:4**	9:4	12:4	13:4
B	0:5	0:0	0:2	0:3	0:6	0:7

calculate a family of three-dimensional structures. Preliminary rounds of calculation were carried out with all possible disulfide connectivities to determine the disulfide connectivities of the peptides that were synthesized without directed formation of the disulfide bonds. When no NOE violations greater than 0.2 and no angle violations greater than 2 were detected, the structures were calculated again using ambiguous distance restraints in X-PLOR version 3.1f.

In the last round of structure calculations hydrogen-bond (H-bond) restraints were included. H-bonds were identified from the slow exchange amide proton information, from prediction by MolMol (40), and by manual measurement of N-H-O angles and NH-O and N-O distances in preliminary structures. The angular and distance requirements of an H-bond were from Creighton (41).

The lowest energy 20 structures for the globular and ribbon peptides were selected. The coordinates of these structures have been deposited at the Protein Data Bank Research Collaboratory for Structural Bioinformatics (1MXN and 1MXP for the native and ribbon isomers, respectively).

Structure Analysis—Consensus motifs and disulfide bond conformations were identified using Promotif-NMR (42). Procheck-NMR was used to further analyze the structures. The program MolMol (40) was used to visualize the molecules and to calculate mean global backbone and mean global heavy atom root mean square deviations (RMSD).

Cell Preparation—Parasympathetic neurons from neonatal (3–8-day-old) rat intracardiac ganglia were isolated and cultured as described previously (43). Briefly, rats were sacrificed by decapitation; the hearts were excised, and the atria were removed and incubated for ~1 h at 37 °C in a saline solution, containing 1 mg/ml collagenase (type 2, Worthington). Following enzymatic treatment, clusters of ganglia were dissected from the epicardial ganglion plexus, and neurons were dispersed by trituration in a high glucose culture medium (Dulbecco's modified Eagle's media, containing 10% (v/v) fetal calf serum, 100 units/ml penicillin, and 0.1 mg/ml streptomycin). Dissociated neurons were plated on to laminin-coated glass coverslips and incubated at 37 °C in a 95% air, 5% CO_2 atmosphere for 24–48 h. For experimentation, coverslips containing dissociated neurons were transferred to a perfusion chamber (0.5 ml volume) mounted on an inverted microscope.

Electrophysiological Recording—Agonist-evoked responses of dissociated parasympathetic neurons were studied using the whole-cell recording configuration of the patch clamp technique. Electrical access to the cell interior was obtained using the perforated patch whole-cell recording configuration (44). A final concentration of 240 μg/ml amphotericin B in 0.4% Me_2SO was used in the pipette solution. Pipettes were pulled from thin wall borosilicate glass (Harvard Apparatus Ltd., Kent, UK) and after fire polishing had resistances of ~1 megohm. Access resistances using the perforated patch configuration were routinely 4–8 megohms before series resistance compensation.

Membrane currents were monitored using an Axopatch 200A patch clamp amplifier (Axon Instruments Inc., Union City, CA), filtered at 2 kHz, then digitized at 10 kHz (Digidata 1200 interface, Axon Instruments Inc.), and stored on the hard disc of a computer for viewing and analysis. Voltage clamp protocols were applied using pClamp software (version 6.1.2, Axon Instruments Inc.). Dose-response curves were fitted using a χ^2 minimization, non-linear curve fitting routine Microcal Origin 6.0 (Microcal Software Inc., Northhampton, MA). Numerical data are presented as the mean ± S.E. (*n*, number of observations).

Solutions and Reagents—The pipette filling solution for perforated patch experiments contained (in mM): 75 K_2SO_4, 55 KCl, 5 $MgSO_4$, and 10 HEPES, titrated with *N*-methyl-D-glucamine to pH 7.2. The control extracellular solution contained (mM): 140 NaCl, 3 KCl, 2.5 $CaCl_2$, 1.2 $MgCl_2$, 7.7 glucose, and 10 HEPES-NaOH (pH 7.2). Acetylcholine (ACh) (500 μM) and atropine (100 nM, to inhibit muscarinic ACh receptor activation) were applied for a duration of 2 s using a rapid Piezo application system to minimize the rapid desensitization of the α7 component of the whole-cell current (45). Toxins were applied to the agonist solution as well as the constant perfusing solution. The time course of solution changes was <5 ms as determined from the change in junction potential upon switching from normal bath solution to one diluted with 2% deionized water. Experiments were carried out at 22 °C. The osmolality of all solutions was monitored with a vapor pressure osmometer (Westcor 5500) and was in the range 280–290 mmol/kg. All chemicals used were of analytical grade. ACh chloride and atropine sulfate were supplied by Sigma.

RESULTS

Peptide Synthesis—The amino acid sequence of α-conotoxin AuIB was assembled using rapid *t*-butyloxycarbonyl amino acid/*O*-benzotriazol-1-yl-*N*,*N*,*N*′,*N*′-tetramethyluronium hexafluorophosphate)/diisopropylethylamine *in situ* neutralization chemistry (46). An average coupling yield of 99.80% (assessed by ninhydrin assay) was achieved. Fully reduced peptide was isolated in high purity after HF cleavage and HPLC purification and characterized using MS. The purified peptide was oxidized using a mixture of 10:1 0.05 M NH_4HCO_3 and isopropyl alcohol to give two isomers, the native (globular) and ribbon isomers, which were purified by HPLC and characterized using MS. The native AuIB isomer was produced in greater yield than the ribbon isomer under the selected oxidation conditions. Quantities of highly purified peptides were obtained for the structural and functional studies.

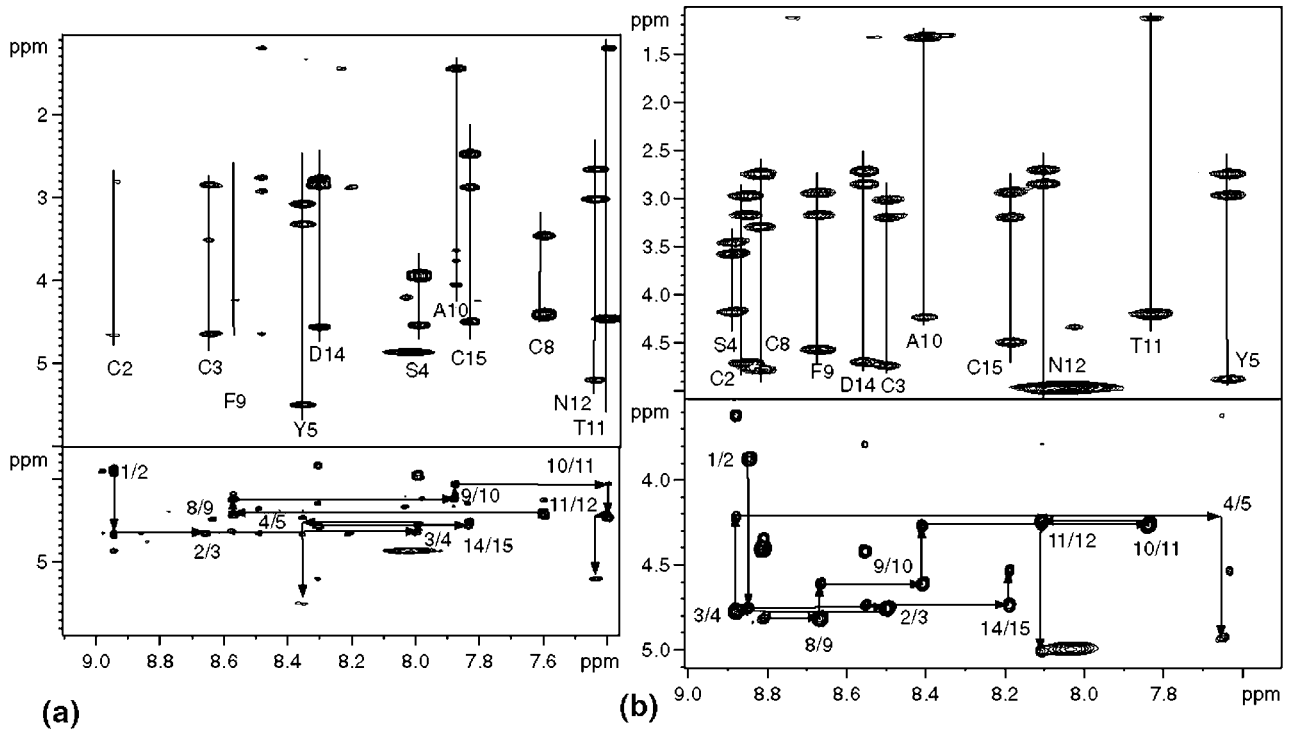

FIG. 2. **Two-dimensional NMR spectra that summarize the sequential assignments for native (*a*) and ribbon AuIB (*b*).** The *lower panels* are parts of NOESY spectra of native or ribbon AuIB in 90% H_2O, 10% D_2O acquired at 290 and 280 K, respectively. The *upper panels* are parts of TOCSY spectra for the same samples. In the *upper panel* the different spin systems are identified. In the *lower panel* the sequential assignment is shown. The abbreviation $i/i + 1$ is used to label the NOE that results from interaction between the α proton of residue i and the backbone amide proton of the following residue.

NMR Data—High quality spectra were obtained for both isomers. The amide signals were spread over the ranges 8.99 to 7.45 and 8.89 to 7.69 ppm for the native and ribbon isomers, respectively. The reasonable dispersion indicates that they adopt ordered structures, with the slightly greater spread of signals for the native form providing a first indication that it adopts the most well defined structure. Sequential assignments were made based on TOCSY, double quantum filtered correlation spectroscopy (DQF-COSY), and nuclear Overhauser effect spectroscopy (NOESY) spectra. Representative spectra showing the assignment of the native and ribbon forms are shown in Fig. 2. Despite the fact that the samples were chemically pure, as judged by MS and HPLC, extra spin systems were present in spectra of the native isomer, suggesting the presence of a second conformation in solution. Because this conformer was of low relative population (<10%), it was not possible to characterize it fully, and subsequent studies focused on the major isomer. The observation of minor conformers in the spectra of small disulfide-rich peptides is not uncommon and may result from cis/trans-isomerization of Pro residues or pro-*R*/pro-*S* disulfide bond configurations. Only peaks corresponding to a single isomer were observed in the spectra of the ribbon isomer.

Chemical shifts were examined to identify which residues in the peptides were involved in secondary structure. The differences between observed and random coil α-proton shifts (referred to as secondary shifts) for the native and ribbon isomers are shown in Fig. 3. From the contiguous sequence of negative secondary shifts from residues Pro-6 to Ala-10, it is clear that the native isomer incorporates a helix over this region. In contrast, the ribbon isomer has a less regular pattern of secondary shifts, indicative of less well defined secondary structure. The fact that the two isomers have quite different structures is exemplified by the large difference in α-proton shifts of Tyr-5 in the two structures, presumably resulting from different relative orientations of the aromatic side chain and subsequently different ring current effects.

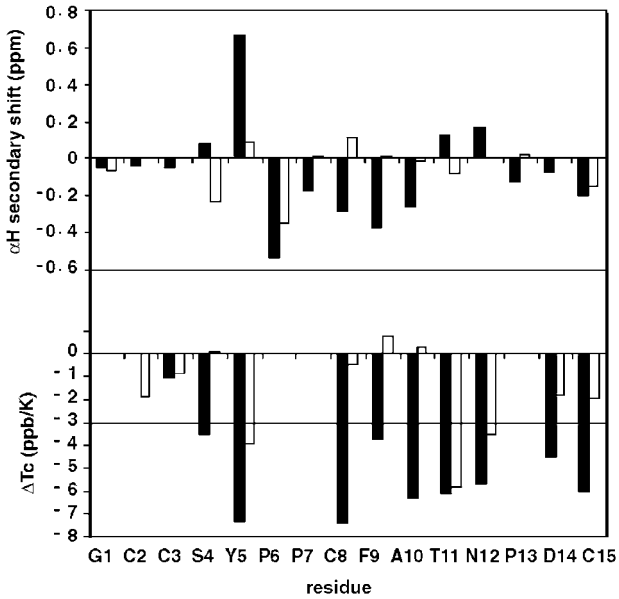

FIG. 3. **Secondary shifts (*top*) and temperature coefficients (*bottom*) for native and ribbon AuIB.** Native AuIB is indicated by the *black bar,* and ribbon AuIB is indicated by the *white bar.* In the *top graph* the differences between the actual shifts of the α protons and their respective random coil shifts are graphed for each residue. A continuous stretch of residues that exhibit negative deviations from random coil indicates helix. A sequence specific correction factor of 0.29 ppm was deducted from residues preceding Pro. In the *bottom graph* a change in temperature coefficient from that for random coil of less than −3 ppb/K indicates residues that may be solvent-protected.

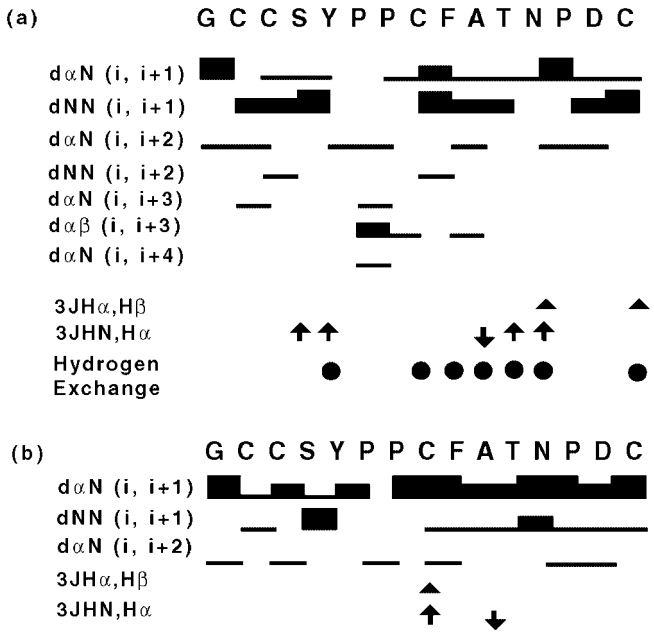

FIG. 4. **Summary of NMR data that defines secondary structure in native and ribbon AuIB.** Data for native AuIB and ribbon AuIB are summarized in the *top* and *bottom panels*, respectively. *Thick*, *medium*, and *thin black bars* indicate strong, medium, and weak NOEs, respectively. *Filled circles* indicate residues that had slowly exchanging amide protons. *Filled triangles* indicate residues for which $^3J_{H\alpha,H\beta}$ couplings were significant. *Up* and *down arrows* indicate large and small $^3J_{HN,H\alpha}$ couplings, respectively. For Pro residues HN refers to the δ protons.

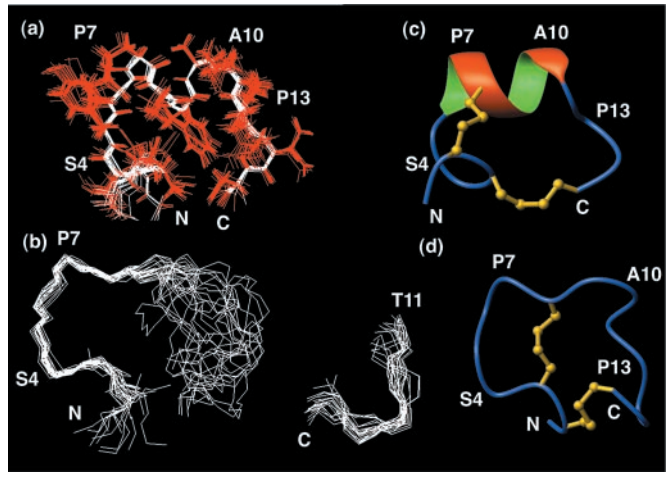

FIG. 5. **Overlay of the 20 lowest energy structures of native AuIB (*a*) and ribbon AuIB structures (*b*) and ribbon depictions of secondary structure of native AuIB (*c*) and ribbon AuIB (*d*).** In the ribbon depictions disulfide bonds are shown as *gold balls* and *sticks*. The overlay of the ribbon structures only shows the backbones of the molecules. In the native AuIB overlay the side chains are shown in *red*. Native AuIB is aligned from residues 2 to 15, and ribbon AuIB is aligned from 2 to 10. *b*, an overlay of just residues 11–15 is also shown. The position of residues 2–10 in relation to residues 11–15 in the ribbon depiction (*d*) is not representative of the whole ensemble.

The variation in amide proton chemical shifts with temperature provides a measure of exposure to solvent, and hence potentially yields information on hydrogen bonding (47, 48). With the exception of Phe-9 all residues from Ser-4 to Cys-15 of the native isomer of AuIB have temperature coefficients less negative than −4 parts per billion (ppb)/K, a standard measure of amide proton protection from solvent. This was not the case for the ribbon isomer of AuIB where only two residues, Thr-11 and Asn-12, had temperature coefficients less negative than −4 ppb/K. As the amide proton temperature coefficients differ greatly for different amino acid residues in random coil peptides, the temperature coefficients for the native and ribbon isomers of AuIB were further considered relative to random coil temperature coefficients. From Ser-4 to Cys-15 in the native AuIB peptide, the temperature coefficients relative to random coil temperature coefficients are smaller than −3 ppb/K (Fig. 3) but greater than −3 ppb/K for other residues. When the data are considered in this way, it appears that the amide proton of Phe-9 in the native isomer of AuIB and amide proton of Tyr-5 of the ribbon isomer of AuIB are also solvent-protected.

The conclusions drawn from the temperature coefficient data are strongly supported by measurement of the exchange rates of amide protons with solvent D_2O. The backbone amide protons of Tyr-5, Cys-8, Phe-9, Ala-10, Thr-11, Asn-12, and Cys-15 were still detected in NMR spectra recorded 4 h after dissolution of the native isomer in D_2O. All backbone amide protons had exchanged in the native isomer after 24 h in D_2O. No backbone amide protons were detected for the ribbon isomer 5 min after dissolution of the peptide in D_2O. This confirms that the native isomer has a substantially more stabilized structure than the ribbon form.

Fig. 4 summarizes NMR data that were used to characterize fully the secondary structures of the native and ribbon AuIB isomers. These include coupling constants that were used to assign dihedral angle restraints, slow exchanging amides that are involved in H-bonds, and a summary of some pertinent NOE restraints. The strong dNN NOEs relative to dαN NOEs in the middle region of the native isomer, for example, suggest the presence of helical structure. The relative intensity of dNN NOEs to dαN NOEs is quite different in the ribbon isomer and is more indicative of an extended structure. Couplings that were used to calculate χ_1 and ϕ angles are also indicated in Fig. 4.

Structure Calculations—Analysis of the NMR spectra for the native isomer yielded a total of 184 NOE restraints including 32 medium and 18 long range NOE restraints. Seven angle restraints were included with the ϕ angles of Ser-4, Tyr-5, Thr-11, and Asn-12 restrained to $-120 \pm 30°$, the ϕ angle of Ala-10 restrained to $-65 \pm 15°$, and the $\chi 1$ angles of Asn-12 and Cys-15 restrained to $180 \pm 30°$. 140 NOE restraints, including 4 long and 13 medium range NOEs, were identified in the NMR spectra of the ribbon isomer. Three dihedral angles were included, with the ϕ angles for Cys-8 and Ala-10 restrained to $-120 \pm 30°$ and $-65 \pm 15°$, respectively, and the $\chi 1$ angle for Cys-8 restrained to $-60 \pm 30°$. These restraints were used to calculate three-dimensional structures for the native and ribbon isomers.

The ensemble of native AuIB structures overlays very well (Fig. 5*a*) with a pairwise backbone RMSD of 0.36 ± 0.13 Å over residues Cys-2 to Cys-15. Table III summarizes the structural and energetic statistics for the calculated structures. The native isomer features an α-helix from Tyr-5 to Asn-12 (Fig. 5*c*) which is flanked by turns. In 6 of 20 structures, a 3_{10} helical region is present in the N-terminal region of the peptide from Gly-1 to Ser-4. The disulfide bond joining Cys-2 and Cys-8 is present in a right-handed hook conformation in 17 of the 20 structures, but there is no consensus configuration for the disulfide between Cys-3 and Cys-15. The average $\chi 2$, $\chi 3$, and $\chi 2'$ angles for the right-handed hook Cys-2 to Cys-8 disulfide bonds are −65, 101, and 141° in 13 structures and −128, 78, and 153° in the other four structures. The average $\chi 2$, $\chi 3$, and $\chi 2'$ angles for the non-right-handed hook Cys-2 to Cys-8 disulfide bonds are 53, −62, and −57°. The structure is stabilized by the presence of hydrogen bonds between the CO groups of Cys-2, Pro-6, Cys-8, Phe-9, and Asn-12 and the NH groups of

TABLE III
Structural and energetic statistics for native and ribbon AuIB

	AuIB native	AuIB ribbon
Mean RMSD from experimental restraints		
NOE (Å)	0.009 ± 0.001	0.025 ± 0.005
Dihedral (°)	0.244 ± 0.141	0.180 ± 0.279
Mean RMSD from Idealized covalent geometry		
Bonds (Å)	0.0058 ± 0.0003	0.0687 ± 0.0011
Angles (°)	2.06 ± 0.04	2.24 ± 0.11
Impropers (°)	0.14 ± 0.02	0.18 ± 0.04
Restraint violations		
NOE violations >0.1Å	0	2.65 ± 1.63
Maximum NOE violation (Å)	0.081	0.197
Dihedral angle violations >1°	0.05 ± 0.22	0.10 ± 0.31
Maximum angle violation (°)	1.2	1.8
Mean energies (kJ mol^{-1})		
E_{NOE}	0.49 ± 0.13	2.76 ± 1.08
E_{cdih}	0.03 ± 0.03	0.00 ± 0.00
E_{vdw}	−62.23 ± 1.75	−45.16 ± 2.42
E_{bond}	1.41 ± 0.10	.87 ± 0.51
$E_{improper}$	0.23 ± 0.06	0.35 ± 0.16
E_{angle}	22.44 ± 0.76	26.52 ± 2.71
E_{total}	−37.64 ± 1.91	−13.66 ± 5.05
Pairwise RMSD		
Backbone atoms (N,Cα,C) (Å)	(2–15) 0.36 ± 0.13	(2–10) 1.08 ± 0.38
	(1–15) 0.65 ± 0.25	(11–15) 1.20 ± 0.50
		(1–15) 2.50 ± 0.73
Heavy atoms (Å)	(2–15) 0.95 ± 0.15	(2–10) 1.69 ± 0.51
	(1–15) 1.04 ± 0.19	(11–15) 2.47 ± 0.87
		(1–15) 3.18 ± 0.80
Ramachandran Plot		
Most favored regions (%)	83.0	56.0
Additional allowed regions (%)	17.0	33.5
Generously allowed regions (%)	0	9.5
Disallowed regions (%)	0	1.0

Tyr-5, Ala-10, Thr-11, Asn-12, and Cys-15, respectively. The CO of Tyr-5 forms a bifurcated hydrogen bond with the NH groups of both Cys-8 and Phe-9.

In contrast with the native form, the individual structures of the ribbon isomer of AuIB do not align well over the whole molecule and have a pairwise backbone RMSD of 2.50 ± 0.73 Å (Fig. 5*b*). The alignment is better over smaller regions within the structure. For example, residues 2–10 overlay with a pairwise backbone RMSD of 1.08 ± 0.38 Å and residues 11–15 overlay with a pairwise backbone RMSD of 1.20 ± 0.50 Å. The global fold is shown in Fig. 5*d*. Whereas there is an overall similarity in the shape of the fold relative to the native isomer, the ribbon isomer lacks a defined helical region. The region that is helical in the native form is straightened out, and the backbone bends over residues Tyr-5 to Pro-7 and at Ala-10 and Pro-13 in the ribbon isomer. The disulfide bond joining Cys-3 and Cys-8 in the ribbon isomer is present in either a right- or left-handed spiral conformation in the individual structures within the ensemble. The average $\chi 2$, $\chi 3$, and $\chi 2'$ angles for the left-handed spiral Cys-2 to Cys-8 disulfide bonds are −114, −83, and −105°. The average $\chi 2$, $\chi 3$ and $\chi 2'$ angles for the right-handed spiral Cys-2 to Cys-8 disulfide bonds are 68, 91, and 135°. There is no consensus conformation for the disulfide bond joining Cys-2 and Cys-15 of the ribbon isomer.

The first loops of the ribbon and native isomers overlay well (Fig. 6), with a mean global backbone RMSD of 0.92 ± 0.00 Å over residues Cys-3 to Cys-8. The second loop of the molecule is "looser" in the ribbon isomer relative to the native. Overlays of the ribbon and native AuIB structures with the structures of related α-conotoxins are also shown in Fig. 6.

Ramachandran plots show the likely ψ and ϕ angle combinations for residues in proteins and are based on the measurement of these angles in 163 known structures. All of the residues in the native isomer (excluding Pro and Gly) lie in the most favored and additionally allowed regions of the Ramachandran plot. 89.5% of the residues in the ribbon isomer (excluding Pro and Gly) were in the most favored and additionally allowed regions, and 9.5% were in the generously allowed regions and 1% in the disallowed regions. The residues that lie in the disallowed regions were not confined to just one or two residues in the ensemble and were distributed over different residues, from Phe-9 to Asn-12 and Cys-2 and Cys-3. A large proportion of Thr-11 residues lay in the generously allowed regions. This is not surprising as Ramachandran statistics are based on angles seen in structures of native proteins and may not necessarily reflect the angles observed in small constrained peptides, particularly those with non-native folds.

Electrophysiology—Rapid focal application of ACh (500 μM) to dissociated neurons of the rat parasympathetic ganglia held at −70 to −80 mV, in the presence of 100 nM atropine, resulted in a characteristic biphasic inward current comprising an initial transient peak that rapidly decayed to a steady-state current (Fig. 7). The ratio of peak to steady-state current amplitude varied between neurons.

Effects of native and ribbon AuIB on nicotinic ACh responses were investigated in 30 neurons. Native AuIB inhibited the ACh-evoked current in a dose-dependent manner in 12 of 14 neurons and ribbon AuIB in 12 of 16 neurons. In the remaining six neurons, the ACh-evoked current was not inhibited in the presence of >1 μM AuIB. This is most likely due to heterogeneity in the expression of the β4 subunit that has been shown using single cell PCR analysis to be expressed in a proportion (>50%) of neurons (49). The half-maximal inhibitory concentration (IC_{50}) value for native AuIB was 1.2 nM and maximal block ranged from 21 to 62% of the total ACh-induced current. The ribbon AuIB isomer had an IC_{50} of 0.1 nM and caused a maximal block of 31–59% of the control current. The inhibition of ACh-evoked currents by the ribbon AuIB isomer was slowly reversible, whereas <50% recovery was obtained after 30 min of washout.

The finding that the ribbon isomer has an activity 10-fold higher than the native was unexpected and to our knowledge

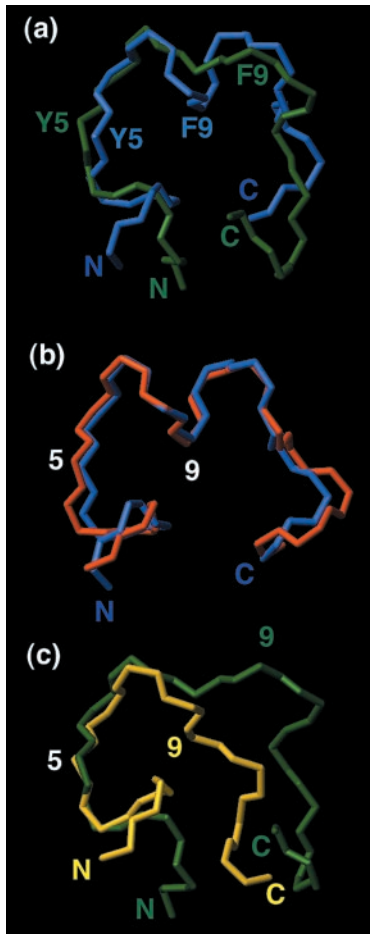

FIG. 6. **Overlays of native and ribbon AuIB (*a*), native AuIB with PnIB (7) (*b*), and ribbon AuIB with ImI (13) (*c*).** Native AuIB is *blue*; ribbon AuIB is *green*; PnIB is *red*; and ImI is *yellow*. Side chains are not shown. Native AuIB and ribbon AuIB are aligned over the backbone atoms of Cys-3 to Cys-8. The position of residues 2–10 in relation to residues 11–15 in ribbon AuIB is not representative of the whole ensemble. AuIB and PnIB are aligned from residues 2–14. AuIB and ImI are aligned over residues 3–8.

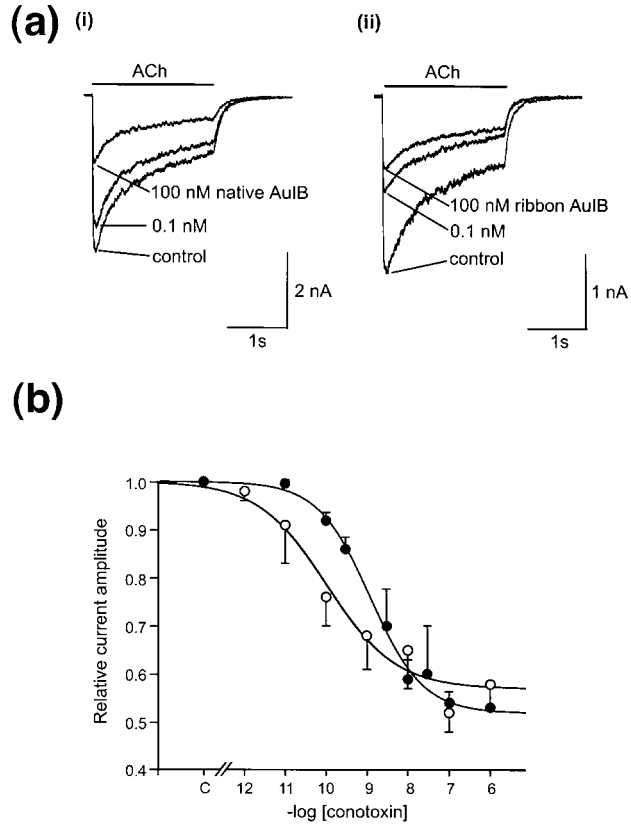

FIG. 7. **Effect of native and ribbon isomers of AuIB on nicotinic ACh-evoked currents in rat parasympathetic neurons.** Rapid application of 500 μM ACh in the presence of atropine (100 nM) evokes a characteristic biphasic response, with an initial peak that rapidly decays to a steady-state level. *a,* superimposed traces of ACh-induced whole-cell currents in the absence (control) and presence of various concentrations of native (*i*) and ribbon (*ii*) isomers of AuIB. Inhibition of the steady-state current was variable; hence, all measurements were of the peak current. Holding potential −70 mV. *b,* concentration-response relationship obtained for the inhibition of the peak ACh-induced current by native (●) and ribbon (○) AuIB isomers. IC_{50} values and Hill coefficients obtained from fitted curve were 1.2 and 0.6 nM and 0.1 and 0.5 nM, respectively, for the native and ribbon isomer.

represents the first observation of an increase in activity being produced by non-native disulfide connectivity in a conotoxin.

DISCUSSION

In the current study, we have synthesized and have determined the three-dimensional solution structures of the ribbon and native forms of α-conotoxin AuIB. Native α-conotoxin AuIB features an α-helical region from Tyr-5 to Asn-12 that is flanked by turns, whereas in the ribbon form the helical nature of AuIB is lost. We have also investigated the potency of the native and ribbon AuIB peptides as antagonists of the nAChRs present in rat parasympathetic neurons and have made the surprising finding that the ribbon isomer is approximately 10 times more potent at this site than native AuIB.

The consensus features of the native AuIB structure described here are similar to those in a recently reported structure (17), with the α-helical region spanning the same residues in both. The two structures are virtually identical in the first loop, but there are some minor changes, over residues 12–14, in the second loop. Comparison of the NOE and angle restraints used in calculation of the two AuIB structures identifies some differences that may explain this structural change. The use of 750 MHz NMR data in our study allowed us to include more medium and long range NOE restraints in the structure calculations than the previous study, which used 600 MHz NMR data. In particular, we included 50 medium and long range NOEs, and the other study included 32 (although they stated 38 in the paper there were 32 in the deposited restraints). Twenty of these NOE restraints were identical, and many of the other restraints although not identical were derived from interactions between the same amino acid residues. The Asn-12 $\chi 1$ angle was restrained in our structure but not in the Cho *et al.* (17) structure. In addition, the Cho *et al.* (17) structure included NOEs between Asn-12 and Cys-15 and between Cys-8 and Thr-11 that were not observed in our spectra. We included NOEs between Phe-9 and Thr-11, Asp-14, and Cys-15 that were not observed by Cho *et al.* (17). These restraint differences explain the observed structural differences, but the origin of the restraint differences is not clear as similar experimental conditions were used. The major difference was that they used a peptide concentration of 6 mM whereas we used 2 mM.

AuIB is a member of the 4/6 family of α-conotoxins, and because it is the only member of this class for which structural information is available, it was of interest to compare its structure with members of other framework classes. Fig. 6*b* shows that the first loop of AuIB overlays well with the representative 4/7 α-conotoxin PnIB. Indeed AuIB features the α-helix that is typical of the 4/7 class. The only significant difference between the structure of AuIB and α-conotoxins from the 4/7 class is that the second loop is tighter in AuIB due to the smaller loop size. The 4/6 α-conotoxin AuIB also overlays well with the 4/3 α-conotoxin ImI over the first loop but exhibits large structural

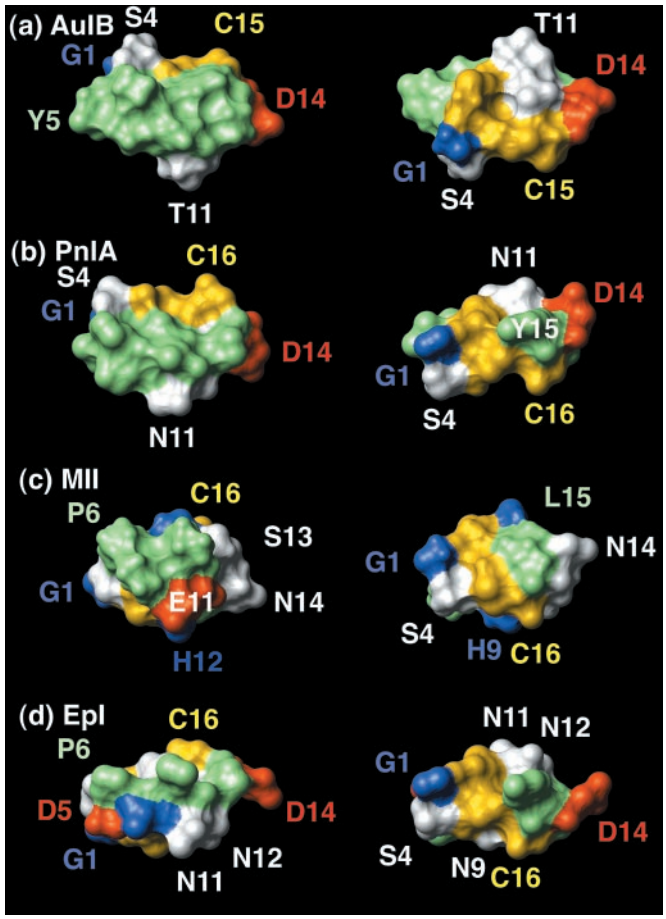

FIG. 8. **Solvent-accessible surfaces of AuIB (*a*), PnIA (8) (*b*), MII (11) (*c*), and EpI (10) (*d*).** Hydrophobic residues are *light green*; positive residues are *blue*; negative residues are *red*; Cys residues are *gold*; and all other residues are *white*. Views on the right-hand side are rotated 180° from the views on the left-hand side.

differences from ImI in the second loop (not shown).

In structures of the 4/7 α-conotoxins determined by x-ray crystallography, PnIA, PnIB, and EpI, a region of 3_{10} helix is observed N-terminal to the α-helix (7, 8, 10). There are no solution structures reported for these molecules, but ImI has the same first loop as EpI, and four independent solution structures of ImI have been reported. An N-terminal 3_{10} helical motif is reported in just one of the four ImI NMR structures (16), and no other NMR structures of α-conotoxins report this element of secondary structure (9, 11–15, 17). In the structure described here a 3_{10} helix is detected in 6 of 20 AuIB structures. It appears that the 3_{10} helix is a nascent element of structure that may be stabilized as the peptides are crystallized.

The general similarity in the backbone fold of the 4/*X* α-conotoxins suggests that an understanding of their varying specificities requires a more detailed examination of the surface properties of the molecules. Fig. 8 shows surface representations of AuIB and of the 4/7 α-conotoxins PnIA, MII, and EpI. An initial comparison of the surface properties of AuIB and PnIA shows that they are quite similar. These peptides, however, show different specificity, binding to α3β4 and α3β2 receptor subtypes, respectively. Both AuIA and AuIC bind to the α3β4 receptor but with less potency than AuIB. They differ from AuIB in having an additional residue in the second loop, Tyr-15, and by having a Ser in position 13 rather than a Pro. Tyr-15 in PnIA is therefore probably not the factor that prevents PnIA from binding to the α3β4 receptor. A closer examination of the surface properties of AuIB and PnIA shows that the distinct large hydrophobic surface in AuIB is smaller and is encroached upon by the nearby polar residues Asn-11 and Cys-16 in PnIA to a greater degree than occurs for the corresponding residues in AuIB. The hydrophobic patch in MII, another α3β2-specific α-conotoxin, is also smaller than in AuIB and encroached upon by polar and charged residues. In EpI, which binds to both α3β4 and α3β2 receptors, the hydrophobic residues form a ridge that protrudes from the surrounding polar and charged residues. Perhaps then the hydrophobic patch in AuIB is important in determining specificity for the β4 subunit over the β2 subunit. EpI may be able to bind to the α3β4 receptor as the ridge of hydrophobic residues are raised above the surrounding polar and charged residues and may be able to interact. There is also the possibility that EpI contacts different residues in the α3β4 receptor than AuIB. This was found to be the case for ImI and PnIA binding to the α7 receptor.

The authors of the other AuIB structure noted that the Asp-14 side chain of AuIB is in a similar position to Tyr-15 in PnIA. This was not found to be the case in our structure of native AuIB, and we therefore believe that a change in the position of Asp-14 in AuIB relative to where it lies in AuIA and AuIC is not likely to be the cause of the observed increased activity in AuIB over AuIA and AuIC. We cannot, however, rule this out because Asp-14 may be in a different position in AuIA and AuIC than it is in PnIA due to the replacement of the Pro-13 in PnIA with a Ser in that position in AuIA and AuIC.

Our NMR studies show that a decrease in structural homogeneity occurs when the connectivities of the disulfide bonds of AuIB are changed from their native form. The disulfide bonds in the ribbon isomer brace the peptide to some extent but not as tightly as in the native isomer. Comparison of the structures shows that the ribbon structure is largely unchanged from the native structure in the first loop of the molecule (Fig. 6). The second loop is very different, being looser than the corresponding loop in the native peptide. This structure is reminiscent of ImI, shown in Fig. 6*c*, where the first loop is identical to members of the 4/7 family but the second loop is significantly altered (13).

The reduction in structural homogeneity that results from altering the disulfide connectivity from the globular to ribbon form provides an insight into the role of the disulfide bonds in defining the structure. The trend in backbone atom pairwise RMSDs between the native and ribbon forms of AuIB is similar to that seen for the native and ribbon forms of GI. In both cases the ribbon isomer is less precisely defined (*i.e.* has higher RMSD values) than the respective native peptide. Increases in RMSD values can result either from a lack of sufficient NOE or dihedral angle restraints or from inherent flexibility. Based on the trends in slow exchange amide protons and temperature coefficients, it appears that the latter is the more likely explanation and that the large RMSD for the ribbon isomer of AuIB reflects a high degree of flexibility in this structure. Thus, the disulfide bonds appear to play a role both in influencing the final shape of the molecule and its dynamic flexibility.

In the case of GI, the ribbon connectivity resulted in a structure that, although relatively well defined, was different from that of the native structure. The inactivity of the ribbon isomer of GI was attributed to its non-native structure and to only a moderate increase in structural flexibility over the native form (22). That was presumed to prevent it from adopting the fold required for binding to the muscle nAChR. It is interesting to note that the ribbon isomer of AuIB is a potent antagonist of nAChRs in dissociated neurons of rat parasympathetic ganglia. The ability of the AuIB ribbon isomer to bind to the neuronal nAChR may reflect greater flexibility in this peptide, as compared with the GI ribbon isomer, allowing it to adopt a conformation that is capable of binding. The greater flexibility of the ribbon isomer of AuIB is

reflected not only in the higher RMSD than GI but also in the fact that it has no slowly exchanging protons at all, whereas Ala-6 is slowly exchanging in the GI ribbon isomer.

A further understanding of the reasons for the activity of the ribbon isomer would be assisted by mutagenesis studies. There are currently no extensive mutagenesis data available in AuIB analogues, but some insight into residues important for binding can be obtained from a comparison of the structure of AuIB and the structure activity relationship data of related α-conotoxins. Residues in PnIB and ImI that interact with the α7 receptor have been identified (50–52). Whereas AuIB binds to the α3β4 receptor rather than the α7 receptor, it is interesting to note that for both PnIB and ImI two of the important residues for binding are on the first loop and one is in the second loop. All of the important residues are in the central region of the peptides, corresponding to the helical region. In the ribbon isomer of AuIB the first loop is essentially unchanged from that in the native. If the suggestion that the residues responsible for the interaction of AuIB with the α3β4 receptor are in similar positions to the residues in PnIB and ImI that interact with the α7 receptor is correct, then binding of ribbon AuIB to the receptor is logical. Residues in the first loop are essentially in the same positions relative to one another as they are in the native isomer. The lack of activity in the GI ribbon isomer and the activity of the AuIB ribbon isomer may also reflect differences in the tolerance of the neuronal and muscle nAChR-binding sites to different antagonist conformations.

It is interesting that despite the apparent flexibility of the ribbon isomer of AuIB, it is more active than the native isomer. It appears that once bound, the ribbon isomer is able to have a highly complementary fit with the receptor site.

This study shows that α-conotoxin function can, in the case of AuIB, be increased through changing the disulfide connectivity to a non-native form. This raises the question as to why the ribbon form is not selected over the globular form in the native venom. Although the possibility that a ribbon form does exist in the native venom cannot be excluded, such a form was not evident in the initial report of the discovery of AuIB (28). However there is a precedent for native ribbon isomers in other small conotoxins. The ribbon isomer appears to be selected as the native form in the recently discovered α-conotoxin MrIA (25–27). The structural data reported here for AuIB suggest that perhaps the ribbon isomer is unlikely to be in the venom due to the fact that it is substantially more flexible and hence perhaps less stable *in vivo* than the globular form. It also should be noted that, although the ribbon form of AuIB is more active than native AuIB on the mammalian peripheral neurons used in this study, this may not be the case for *Conus aulicus* prey species. This study does demonstrate, however, that altering disulfide connectivity may in some circumstances be an effective way to increase activity of a peptide.

Acknowledgment—The Institute for Molecular Bioscience is a Special Research Centre of the ARC.

REFERENCES

1. Olivera, B. M. (1997) *Mol. Biol. Cell* **8,** 2101–2109
2. Adams, D. J., Alewood, P. F., Craik, D. J., Drinkwater, R. D., and Lewis, R. J. (1999) *Drug Dev. Res.* **46,** 219–234
3. Olivera, B. M. (1999) *J. Comp. Physiol.* **185,** 353–359
4. McIntosh, J. M., Santos, A. D., and Olivera, B. M. (1999) *Annu. Rev. Biochem.* **68,** 59–88
5. McIntosh, J. M., Gardner, S., Luo, S., Garrett, J. E., and Yoshikami, D. (2000) *Eur. J. Pharmacol.* **393,** 205–208
6. Dutton, J. L., and Craik, D. J. (2001) *Curr. Med. Chem.* **8,** 327–344
7. Hu, S., Gehrmann, J., Alewood, P. F., Craik, D. J., and Martin, J. L. (1997) *Biochemistry* **36,** 11323–11330
8. Hu, S., Gehrmann, J., Guddat, L. W., Alewood, P. F., Craik, D. J., and Martin, J. L. (1996) *Structure* **4,** 417–423
9. Shon, K., Koerber, S. C., Ricier, J. E., Olivera, B. M., and McIntosh, J. M. (1997) *Biochemistry* **36,** 15693–15700
10. Hu, S., Loughnan, M., Miller, R., Weeks, C., Blessing, R. H., Alewood, P. F., Lewis, R. J., and Martin, J. L. (1998) *Biochemistry* **37,** 11425–11433
11. Hill, J. M., Oomen, C. J., Miranda, L. P., Bingham, J., Alewood, P. F., and Craik, D. J. (1998) *Biochemistry* **37,** 15621–15630
12. Franco, A., and Mari, F. (1999) *Lett. Pept. Sci.* **6,** 199–207
13. Gehrmann, J., Daly, N. L., Alewood, P. F., and Craik, D. J. (1999) *J. Med. Chem.* **42,** 2364–2372
14. Gouda, H., and Hirono, S. (1999) *Biochim. Biophys. Acta* **1431,** 384–394
15. Maslennikov, I. V., Shenkarev, Z. O., Zhmak, M. N., Ivanov, V. T., Methfessel, C., Tsetlin, V. I., and Arseniev, A. S. (1999) *FEBS Lett.* **444,** 275–280
16. Rogers, J. P., Luginbuhl, P., Shen, G. S., McCabe, R. T., Stevens, R. C., and Wemmer, D. E. (1999) *Biochemistry* **38,** 3874–3882
17. Cho, J.-H., Mok, K. H., Olivera, B. M., McIntosh, J. M., Park, K.-H., and Han, K.-H. (2000) *J. Biol. Chem.* **275,** 8680–8685
18. Kaerner, A., and Rabenstein, D. L. (1999) *Biochemistry* **38,** 5459–5470
19. Hashimoto, K., Uchida, S., Yoshida, H., Nishiuchi, Y., Sakakibara, S., and Yukari, K. (1985) *Eur. J. Pharmacol.* **118,** 351–354
20. Almquist, R. G., Kadambi, S. R., Yasuda, D. M., Weitl, F. L., Polgar, W. E., and Toll, L. R. (1989) *Int. J. Peptide Protein Res.* **34,** 455–462
21. Mok, K. H., and Han, K.-H. (1999) *Biochemistry* **38,** 11895–11904
22. Gehrmann, J., Alewood, P. F., and Craik, D. J. (1998) *J. Mol. Biol.* **278,** 401–415
23. Zhang, R., and Snyder, G. H. (1991) *Biochemistry* **30,** 11343–11348
24. Zhang, R. M., and Snyder, G. H. (1989) *J. Biol. Chem.* **264,** 18472–18479
25. Sharpe, I. A., Gehrmann, J., Loughnan, M. L., Thomas, L., Adams, D. A., Atkins, A., Palant, E., Craik, D. J., Adams, D. J., Alewood, P. F., and Lewis, R. J. (2001) *Nat. Neurosci.* **4,** 902–907
26. Balaji, R. A., Ohtake, A., Sato, K., Gopalakrishnakone, P., Kini, R. M., Seow, K. T., and Bay, B. H. (2000) *J. Biol. Chem.* **275,** 39516–39522
27. McIntosh, J. M., Corpuz, G. O., Layer, R. T., Garrett, J. E., Wagstaff, J. D., Bulaj, G., Vyazovkina, A., Yoshikami, D., Cruz, L. J., and Olivera, B. M. (2000) *J. Biol. Chem.* **275,** 32391–32397
28. Luo, S., Kulak, J. M., Cartier, G. E., Jacobsen, R. B., Yoshikami, D., Olivera, B. M., and McIntosh, J. M. (1998) *J. Neurosci.* **18,** 8571–8579
29. Rance, M., Sorensen, O. W., Bodenhausen, G., Wagner, G., Ernst, R. R., and Wuthrich, K. (1983) *Biochem. Biophys. Res. Commun.* **117,** 479–485
30. Griesinger, C., Sorensen, O. W., and Ernst, R. R. (1987) *J. Magn. Reson.* **75,** 474–492
31. Bax, A., and Davis, D. G. (1985) *J. Magn. Reson.* **65,** 355–360
32. Jeener, J., Meier, B. H., Bachmann, P., and Ernst, R. R. (1979) *J. Chem. Phys.* **71,** 4546–4553
33. Kumar, A., Ernst, R. R., and Wuthrich, K. (1980) *Biochem. Biophys. Res. Commun.* **95,** 1–6
34. Clore, G. M., Brunger, A. T., Karplus, M., and Gronenborn, A. M. (1986) *J. Mol. Biol.* **191,** 523–551
35. Williamson, M. P., Havel, T. F., and Wüthrich, K. (1985) *J. Mol. Biol.* **182,** 295–315
36. Wüthrich, K. (1986) *NMR of Proteins and Nucleic Acids*, pp. 176–199, Wiley-Interscience, New York
37. Brünger, A. T., Clore, G. M., Gronenborn, A. M., and Karplus, M. (1986) *Proc. Natl. Acad. Sci. U. S. A.* **83,** 3801–3805
38. Brünger, A. T. (1992) *X-PLOR: A System for X-ray Crystallography and NMR*, Version 3.1, Yale University, New Haven
39. Felizmenio-Quimio, M. E., Daly, N. L., and Craik, D. J. (2001) *J. Biol. Chem.* **276,** 22875–22882
40. Koradi, R., Billeter, M., and Wuthrich, K. (1996) *J. Mol. Graphics* **14,** 29–32 and 51–55
41. Creighton, T. E. (1993) *Proteins, Structures, and Molecular Properties,* 2nd Ed., pp. 133–157, W. H. Freeman & Co., New York
42. Hutchinson, E. G., and Thornton, J. M. (1996) *Protein Sci.* **5,** 212–220
43. Fieber, L. A., and Adams, D. J. (1991) *J. Physiol. (Lond.)* **434,** 215–237
44. Rae, J., Cooper, K., Gates, P., and Watsky, M. (1991) *J. Neurosci. Methods* **37,** 15–26
45. Zhang, Z. W., Vijayaraghavan, S., and Berg, D. K. (1994) *Neuron* **12,** 167–177
46. Schnolzer, M., Alewood, P., Jones, A., Alewood, D., and Kent, S. B. (1992) *Int. J. Pept. Protein Res.* **40,** 180–193
47. Merutka, G., Dyson, H. J., and Wright, P. E. (1995) *J. Biomol. NMR* **5,** 14–24
48. Andersen, N. H., Neidigh, J. W., Harris, S. M., Lee, G. M., Liu, Z., and Tong, H. (1997) *J. Am. Chem. Soc.* **119,** 8547–8561
49. Poth, K., Nutter, T. J., Cuevas, J., Parker, M. J., Adams, D. J., and Luetje, C. W. (1997) *J. Neurosci.* **17,** 586–596
50. Quiram, P. A., and Sine, S. M. (1998) *J. Biol. Chem.* **273,** 11007–11011
51. Quiram, P. A., Jones, J. J., and Sine, S. M. (1999) *J. Biol. Chem.* **274,** 19517–19524
52. Quiram, P. A., McIntosh, J. M., and Sine, S. M. (2000) *J. Biol. Chem.* **275,** 4889–4896
53. Gray, W. R., Luque, A., Olivera, B. M., Barrett, J., and Cruz, L. J. (1981) *J. Biol. Chem.* **256,** 4734–4740
54. Martinez, J. S., Olivera, B. M., Gray, W. R., Craig, A. G., Groebe, D. R., Abramson, S. N., and McIntosh, J. M. (1995) *Biochemistry* **34,** 14519–14526
55. Fainzilber, M., Hasson, A., Oren, R., Burlingame, A. L., Gordon, D., Spira, M. E., and Zlotkin, E. (1994) *Biochemistry* **33,** 9523–9529
56. Loughnan, M., Bond, T., Atkins, A., Cuevas, J., Adams, D. J., Broxton, N. M., Livett, B. G., Down, J. G., Jones, A., Alewood, P. F., and Lewis, R. J. (1998) *J. Biol. Chem.* **273,** 15667–15674
57. Cartier, G. E., Yoshikami, D., Gray, W. R., Luo, S., Olivera, B. M., and McIntosh, J. M. (1996) *J. Biol. Chem.* **271,** 7522–7528
58. McIntosh, J. M., Yoshikami, D., Mahe, E., Nielsen, D. B., Rivier, J. E., Gray, W. R., and Olivera, B. M. (1994) *J. Biol. Chem.* **269,** 16733–16739
59. Rigby, A. C., Lucas-Meunier, E., Kalume, D. E., Czerwiec, E., Hambe, B., Dahlqvist, I., Fossier, P., Baux, G., Roepstorff, P., Baleja, J. D., Furie, B. C., Furie, B., and Stenflo, J. (1999) *Proc. Natl. Acad. Sci. U. S. A.* **96,** 5758–5763

A New Level of Conotoxin Diversity, a Non-native Disulfide Bond Connectivity in α -Conotoxin AuIB Reduces Structural Definition but Increases Biological Activity

Julie L. Dutton, Paramjit S. Bansal, Ron C. Hogg, David J. Adams, Paul F. Alewood and David J. Craik

J. Biol. Chem. 2002, 277:48849-48857.
doi: 10.1074/jbc.M208842200 originally published online October 9, 2002
